Sigma J Eng & Nat Sci 37 (3), 2019, 737-746

Sigma Journal of Engineering and Natural Sciences
Sigma Mühendislik ve Fen Bilimleri Dergisi

Research Article

AN EXPERIMENTAL STUDY ON DETECTING AND IMAGING CAVITY REGIONS INSIDE TREE TRUNK USING CIRCULAR BACK PROJECTION FOCUSING ALGORITHM

Serhat GÖKKAN*[1], Betül YILMAZ[2], Caner ÖZDEMİR[3]

[1]*Dept. of Electrical and Electronics Eng., Mersin University, MERSİN;* ORCID: 0000-0002-2390-9511
[2]*Dept. of Electrical and Electronics Eng., Mersin University, MERSİN;* ORCID: 0000-0001-7404-8312
[3]*Dept. of Electrical and Electronics Eng., Mersin University, MERSİN;* ORCID: 0000-0003-2615-4203

Received: 09.01.2019 Revised: 12.02.2019 Accepted: 01.04.2019

ABSTRACT

In this work, we have presented experimental study for detecting cavity regions inside a tree trunk using circular back projection focusing algorithm (CBPA). First, the validity of CBPA was questioned and then checked by the help of a simulation scenario that were generated using perfect point-scatterers in Matlab programming environment. After achieving perfect reconstruction of the simulated cavity structure together with the tree-body in the simulated scenario, the implementation of CBPA was applied to a real tree-interior imaging radar (TIIR) experiments that were conducted in the laboratory. The resultant focused TIIR radar images of measured data have demonstrated that CBPA can be a strong candidate and successfully utilized for migrating the raw backscattered data for TIIR applications.
Keywords: Remote sensing, radar imaging, tree-penetrating radar, signal processing, back-scattered measurements.

1. INTRODUCTION

The decayed trees cause severe incidents by falling onto people, houses and cars every year [1-2]. It is no doubt that early detection of voids and cavities inside tree structures can help avoiding such undesired incidents. Although most of trees are seen healthy and strong from outside, they usually decay from inside due to worms, insects and small animals that causes significantly big cavities inside the tree body. Various researchers have suggested different methods to detect such voids based on conventional techniques such as acoustic imaging procedures [3], resistivity measurement methods [4], and thermographic inspection [5]. Ultrasonic tomography [6-7]; for example, have the ability of sensing the cavities within the tree bodies; but, it has the disadvantage of having the weak ultrasonic signals such that can only a small proportion of the source signal can penetrate the tree body. To ensure the required minimum detectable signal level, many receivers are required to be put along the perimeter of tree body. Microwave imaging techniques; on the other hand, overcomes the above-mentioned disadvantage by using the radar hardware and employing radar signal processing techniques to enhance the power of the

* Corresponding Author: e-mail: sgokkan@mersin.edu.tr, tel: (324) 361 00 01 / 16778

detectable signal level. In fact; microwave imaging techniques requires smaller amount of power figures to penetrate such obstacles while providing much better resolution. Furthermore, only one transmitter and one receiver are enough to configure the data collection arrangement. Especially, ground penetrating radar (GPR) [8-9] and through the wall imaging radar (TWIR) [10-11] technologies provide similar penetration problems and associated focusing routines that can also be utilized in TIIR problems. Redding and his friends; for instance, has utilized circular measurement set-up to collect the scattered electric field data from a tree trunk and they applied famous circular radon transform method to focus and detect the cavity inside the tree-body [12].

In this work, an implementation of tree-interior imaging is modelled by engaging the circular back projection algorithm (CBPA) to the scattered electric field data such that cavity locations determined accordingly. CBPA is a powerful focusing algorithm that was previously successfully applied in various fields such as imaging the buried targets in GPR applications [13-14] and detecting/imaging breast tumor [15-16]. In this paper, we specially tailor the CBPA to the tree cavity detection problem throughout this study. BPA is employed in the literature for linear data collection set-up. In this work, we are improving BPA for circular data collection configuration such that circular implementation of BPA is developed thru this study. CBPA which we have developed and implemented for the tree trunk interior imaging processes electromagnetic scattering data faster and more practical than other focusing methods such as circular radon transform [12] and sinusoidal template-based focusing [17]. Radon transform focusing algorithm uses projection data associated with cross section of an object. On the other hand; the calculation time is quite long while forming a focusing TIIR image. Likewise, sinusoidal template-based focusing method adds all the data under the template vector that is also not computationally efficient. Therefore; both algorithms are not fast and therefore; not that practical while employing the application.

The organization of this paper is as follows: Section II explains the geometry of our TIIR problem by presenting the back-scattered electric field data collection methodology and giving the details of CBPA used for TIIR configuration. In the third section, a simulation scenario is formed by modelling the tree body with cavities. After acquiring the simulation data in Matlab, the proposed imaging algorithm is tested with the generated simulation data. In the following section, TIIR measurement results from a test-bed with real tree-body with cavity are presented. Our algorithm is applied to the measured data and the corresponding CBPA images of the tree-cavity are provided. Resultant radar images of both the simulation and the measurement data confirm the effectiveness and the success of the suggested algorithm. The last section is devoted to the conclusion of the work and discussions about the usage of CBPA for future tree-interior radar applications.

2. IMAGING/FOCUSING ALGORITHM FOR TIIR

2.1. IMAGING TREE TRUNK'S INTERIOR

A general scenario for tree trunk imaging is illustrated in Fig.1. A highly directive antenna scans tree trunk circularly for the measurement of *M* distinct look-aspects so that whole azimuth angles are taken into account. The radius of the scanning circle is labelled as R_o. The frequency-diverse back-scattered electric-field data are collected in the monostatic configuration of the radar. For any point scatterer $P(x_n, y_n)$ that was assumed to be on the perimeter of the cavity within the radius R_o; therefore, one-dimensional (1D) electric-field data can be approximated by the antenna of the i*th* position as

$$E_i^s(k, \phi) \cong A_i \cdot \exp(-j2kR_i) \quad (1)$$

Here, A_i is the back-scattered electric field amplitude, $R_i = sqrt[(x_i - x_n)^2 + (y_i - y_n)^2]$ is the distance between the antenna and the scatterer, and k is the wavenumber. The above equation

is approximately true provided with the following assumptions: First, the reflection from the tree-trunk's outer shell is range gated and the multi-paths inside the possible inhomogeneous tree-body medium are ignored. Secondly, isotropic radiation within the tree-body geometry is assumed such that the electromagnetic wave propagates within the tree body in a planar manner. Furthermore, the common point-scattering model [18-20] is utilized for the radar imaging application of the tree body and cavity. With this construct, the perimeter of the cavity can be assumed to be constructed by a finite number of point scatterers such that Eqn. (1) can be converted to a summation as given below:

$$\boldsymbol{E^s(k,\phi)} = \sum_{i=1}^{M} A_i \, exp(-j2\boldsymbol{kR_i}) \tag{2}$$

Here, Eqn.(2) ensures a two-dimensional (2D) back-scattered data by considering different look angles of $\boldsymbol{\phi}$ for a finite number of point scatterers (M) that form the tree-body. In this equation, $\boldsymbol{R_i} = sqrt[(\boldsymbol{X} - x_n)^2 + (\boldsymbol{Y} - y_n)^2]$ is the distance vector between all the positions of radar for whole azimuth observation angles of $\boldsymbol{\phi}$ ranging from 1 to M and the scatterer, $\boldsymbol{k}$ is the wave number vector for the stepped frequencies for a total of K distinct frequencies. Then, $\boldsymbol{X}$ and $\boldsymbol{Y}$ vectors correspond to Cartesian coordinates of M antenna positions accordingly as defined below:

$$\begin{aligned} \boldsymbol{X} &= R_0 cos\boldsymbol{\phi} \\ \boldsymbol{Y} &= R_0 sin\boldsymbol{\phi} \end{aligned} \tag{3}$$

Then, the 2D range-angle data, $\boldsymbol{E^s(r,\phi)}$ can easily be provided by taking the 1D inverse Fourier transform (IFT) of Eqn. (2) along the spatial frequency axis. In this data, the point scatterer $P(x_n, y_n)$ exhibits a sinusoidal behavior in the 2D $\boldsymbol{E^s(r,\phi)}$ data for the azimuth angle ($\boldsymbol{\phi}$) variation due to circular scanning during the data collection process. After obtaining the 2D range-angle back-scattered data; $E^s(r,\phi)$, the CBPA [12] can be usefully applied to migrate sinusoidally degraded signatures to focused point-like behaviors that should coincide with the perimeter of the tree-cavity. As result, focused image features can be attained so that cavity regions inside tree trunk are detected and identified.

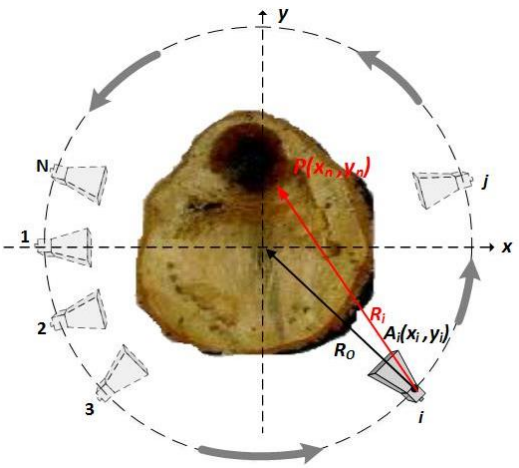

Figure 1. General scenario for tree trunk imaging problem

2.2. IMPLEMENTATION OF CBPA FOR TIIR APPLICATION

Our implementation of CBPA for imaging interior of tree trunk is explained as in the given order: First, a finite number of A-scans [21] of the geometry is gathered for total of M look-

angles. These A-scan vectors are put aside to construct a 2D range-angle image that suffers sinusoidal dispersion. Secondly, a polar to Cartesian transformation routine for the whole data-set is needed since the 2D range-angle data was collected on a polar grid and it needs to be transferred to a uniformly-sampled Cartesian one to be able to utilize the advantages of fast Fourier transform. Prior to this step, an up-sampling procedure also needs to be applied to reduce the noise and the error due to reformatting procedure. Such an interpolation scheme; thus, ensures for a smoother and cleaner image outcome after the migration procedure.

For the implementation of CBPA for our problem, the geometry in Fig. 1 is considered. A radar antenna located at a range distance of R_0 from the center of the tree body transmits a wideband at each look angle M for full azimuth coverage of 360°. The relative permittivity of the tree trunk is denoted by ε_r and the reflectivity function of the scatterers is represented by $e(x,y)$. The instantaneous location of the radar antenna (x_i, y_i) is defined by a unit vector $\overrightarrow{u_i}$ pointing from the center of the scene towards (x_i, y_i) point. The corresponding view angle $\emptyset_i$ is defined as the angle between the unit vector $\overrightarrow{u_i}$ and the x-axis. Assuming a stepped frequency continuous waveform (SFCW) radar signal, the back-scattered signal at a specific view angle can be written as

$$S_{\emptyset_i} = \int_{-\infty}^{\infty}\int_{-\infty}^{\infty} e(x,y)\exp(-jk_r r_i)\mathrm{d}x\mathrm{d}y \tag{4}$$

where k_r is the wavenumber defined for the two-way electromagnetic wave propagation as $k_r = 4\pi f/v$, f is the instantaneous frequency, v is the speed of the propagated wave inside the tree body and r_i is the range from the instantaneous antenna location (x_i, y_i) to the points (x_n, y_n) within the imaging scene. For each look angle, the range profile of the illuminated scene can be found by applying 1D IFT to Eq. (4) and can be mathematically expressed as

$$S_{\emptyset_i}(r) = \mathrm{IFT}\{S_{\emptyset_i}(k_r)\} = \int_{-\infty}^{\infty}\int_{-\infty}^{\infty} e(x,y)\delta(r_i - r)\mathrm{d}x\mathrm{d}y \tag{5}$$

which is also known as the Radon transform of the scene for that particular look angle. The derivation of the back-projection algorithm begins with the IFT expression of the reflectivity function $e(x,y)$written in Cartesian coordinates as

$$e(x,y) = \int_{-\infty}^{\infty}\int_{-\infty}^{\infty} E(k_x, k_y)\exp[j(k_x x + k_y y)]\mathrm{d}k_x\mathrm{d}k_y \tag{6}$$

where $E(k_x, k_y)$ is the 2D FT of $e(x,y)$ Eq. (6) can be modified to be rewritten in the polar coordinates $(k_r, \emptyset_i)$ as follows

$$e(x,y) = \int_{-\pi}^{\pi}\int_{0}^{\infty} E(k_r, \emptyset_i)\exp(jk_r r_i)k_r\mathrm{d}k_r\mathrm{d}\emptyset_i \tag{7}$$

Now, the projection-slice theorem [22] can be used to relate the Fourier transform of the target's reflectivity; $E(k_x, k_y)$ to the available measured data $S_{\emptyset}(k_r)$. For the 2D space, the theorem fundamentally declares that 1D FT of the projection at the angle $\emptyset$ represents the slice of the 2D Fourier transform of the projected (original) scene at the same angle; i.e., $S_{\emptyset}(k_r) \equiv E(k_r, \emptyset)$. Hence, the sampled versions of $E(k_x, k_y)$ can be attained from the FT of the projections $S_{\emptyset}(k_r)$ measured at various observation angles. Using this principle, Eq. (7) can be written as

$$e(x,y) = \int_{-\pi}^{\pi}\left[\int_{0}^{\infty} S_{\emptyset_i}(k_r)\exp(jk_r r_i)k_r\mathrm{d}k_r\right]\mathrm{d}\emptyset_i \tag{8}$$

The bracketed integral in Eq. (8) can be regarded as the 1D IFT of a function of $Q_{\emptyset_i}(k_r) = S_{\emptyset_i}(k_r)k_r$ assessed at r_m. Constituting $q_{\emptyset_i}(r)$ as the IFT of this function, Eq. (8) can be characterized as

$$\mathrm{g}(x,y) = \int_{-\pi}^{\pi} q_{\emptyset_i}(r_i)\mathrm{d}\,\emptyset_i \tag{9}$$

Eq. (9) is the final focused image after the CBPA. For the SFCW system, the implementation of the algorithm can be summarized as follows;

i. Pre-allocate an image matrix of zeros $e(x, y)$ to hold the reflectivity values of the scene.
ii. Multiply the acquired spatial frequency data $S_{\emptyset_i}(k_r)$ with k_r.
iii. Take 1D IFT of (ii) to obtain $q_{\emptyset_i}(r)$ which represents the filtered version of the range profile $s_{\emptyset_i}(r)$.
iv. For each pixel location in the image, compute the corresponding range value r_i and obtain its $q_{\emptyset_i}(r_i)$ value by properly applying an interpolation scheme.
v. Add interpolated values to $e(x, y)$.
vi. Repeat steps (ii) thru (v) for all the observation angles $\emptyset_i$.

3. SIMULATION RESULTS

Our tree interior imaging technique is first checked with a simulation scenario in Matlab programming language with perfect point scatterers. The geometry of the test model is given in Fig. 2. The assumptions listed in the previous section are valid for this experiment. To be able to test and evaluate the performance of this technique with ideal conditions, perimeter of the tree-body (shown as black dots) were assumed to be composed of 120 distinct perfect point reflectors with the identical reflectivity amplitudes of "1" that is also assumed to be independent of frequency and aspect. The radius of the tree body is taken as 40 cm. In the simulation, there were three cavity regions; the first one is centered at $(20\ \text{cm}, -5\text{cm})$, the second one is located at $(-20\ \text{cm}, -10\ \text{cm})$ and the third one is located at $(-5\text{cm}, 15\ \text{cm})$. All cavities were considered to be in the form of circles with diameters of 7 cm, 8 cm and 9 cm for the first, the second and the third void regions, respectively. The circumferences of the cavities were also assumed to be composed of perfect point scatterers with an equal electromagnetic reflectivity of "0.5" that were also assumed to be independent of frequency and angle. Dielectric constant for the tree body is taken as 1.65 that is common for dry tree bodies and assumed to be homogeneous within the tree body. Then, the antenna was moved along a circular track for a total of 360 distinct look-angles to collect the backscattered data.

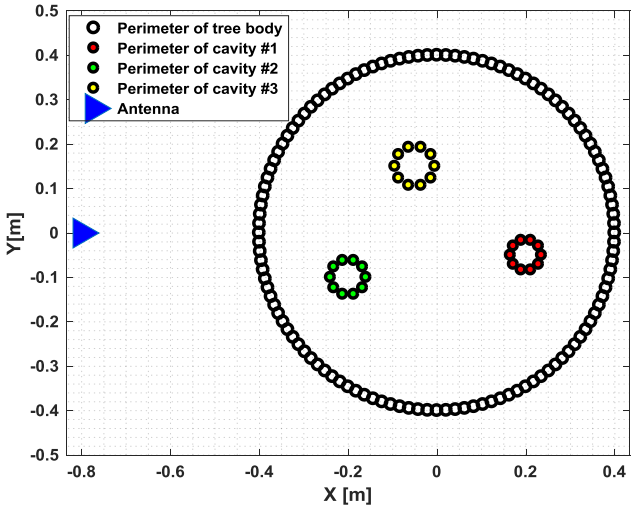

Figure 2. Simulation geometry for tree trunk imaging algorithm

For each of the look angle, frequency-diverse backscattered electric field is gathered for the stepped frequencies ranging from 1 to 8 GHz. for the total of 100 discrete frequency points.

Therefore, the backscattered electric field data is collected on the 2D frequency-angle plane such that a matrix of 100×360 data points is obtained.

The range profile matrix for different look angles; $\boldsymbol{E^s(r,\phi)}$ is obtained by taking the inverse Fourier transform of the backscattered electric field data matrix. For the simulation, $\boldsymbol{E^s(r,\phi)}$ is depicted in Fig. 3(a). We have several observations about the raw range-angle data in Fig. 3(a) as follows: (i) The straight-line scattering is seen from nearest point of circular tree-body geometry because both the scanning path and the tree-body are in the form of circles. This line occurred at a range distance of 40 cm as expected. (ii) Scatterers on the perimeter of the all cavities forms sinusoidal signatures due to different round-trip distances between the antenna and the scatterers' locations. In fact, the peak amplitudes of these oscillating sinusoids depend on their distances from the center of rotation. For the simulation example, these numbers are 3.5 cm, 4 cm and 4.5 cm for the first, the second and the third cavity, respectively. The range-angle image in Fig. 3 (a) exactly exhibits this behavior as we have anticipated. (iii) From the figure, the widths of the sinusoidal behaviors are 7 cm, 8 cm and 9 cm that are precisely the same values of real diameters for the cavity regions. (iv) The starting point of the sinusoidal behavior actually pinpoints the exact location of the cavity: For example, if the sinusoids start from the maximum value, the cavity is located at the nearest point to the antenna's location. If the sinusoid starts from the minimum value; then, the cavity is at 180° away from the antenna. (v) Center point of the scanning will show up as a straight line in the range-angle image. Therefore, if there is a small cavity at the center, its image will be a horizontal line at the half wave between the scatterings from near and far points of the tree body. (vi) Second straight line around 120 cm in range-angle image in Fig. 3(a) corresponds to scattering from far-most point of tree-body. As the radar moves around a circle, the distance from the far-most point of the tree-body stays constant at 120 cm as it was obtained in Fig. 3(a). After analyzing the range-angle image in Fig. 3 (a) that certainly tells us many facts, we applied the CPBA such that the final focused image $\boldsymbol{I(x,y)}$ was obtained as given in Fig. 3(b). As it is clearly seen from the figure, both the tree-body and the cavity regions were successfully imaged in the resultant focused image at their correct locations in the Cartesian coordinates. Of course, the image intensities of cavities are much smaller than those of tree's surface due to decaying of electromagnetic wave with $1/(4\pi R^2)$ term.

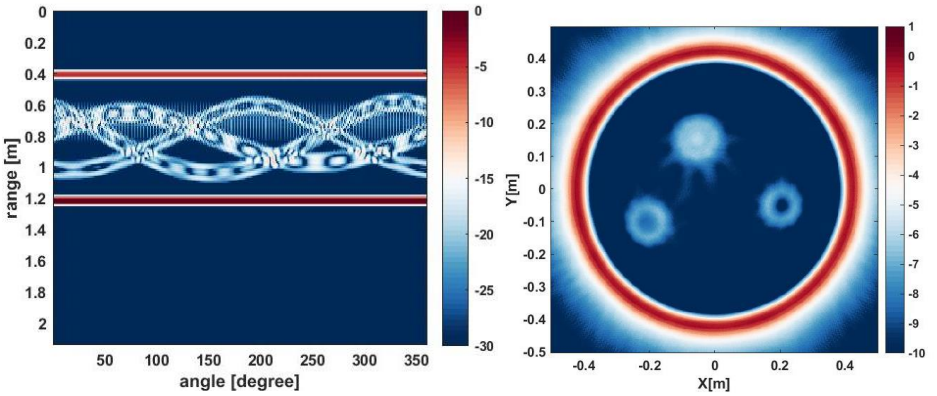

Figure 3. (a) Unfocused image $E^s(r,\phi)$, (b) focused image; after applying CBPA

4. MEASUREMENT SET-UP AND EXPERIMENTAL RESULTS

A measurement set-up has been constructed in our anechoic chamber of Mersin University's Advanced Technologies Research Center (MEATRC) facility to evaluate the effectiveness of our

TIIR detection/imaging algorithm with real experimental data. The geometry of the measurement set-up is shown in Fig. 4. In this set-up, a Vector Network Analyzer (VNA) [Agilent ENA5071B] which can operate between 300 kHz and 8.5 GHz was used to generate/transmit/receive the radar signal by using an ultra-wide band (UWB) double-ridged horn antenna [Geozondas GZ0126DRH] that was used in the monostatic configuration. The values of the antenna parameters were given in Table 1. A turn-table with an automation software was used to get different look-angle profiles of the tree-body. Also, a PC has to be used to synchronously control the VNA and the turn-table with a Matlab [23] script.

Table 1. Parameters of the antenna

Antenna Parameters	Value
Type	Double-Ridged Horn Antenna
Frequency range	1-26 GHz
Gain @ 1 / 8 / 26 GHz	-1.2 dBi / +16 dBi / +20 dBi
E-plane HPBW @ 1 / 8 / 26 GHz	37.7°/ 22.4° / 12.3°
Transmitted power	+5 dBm

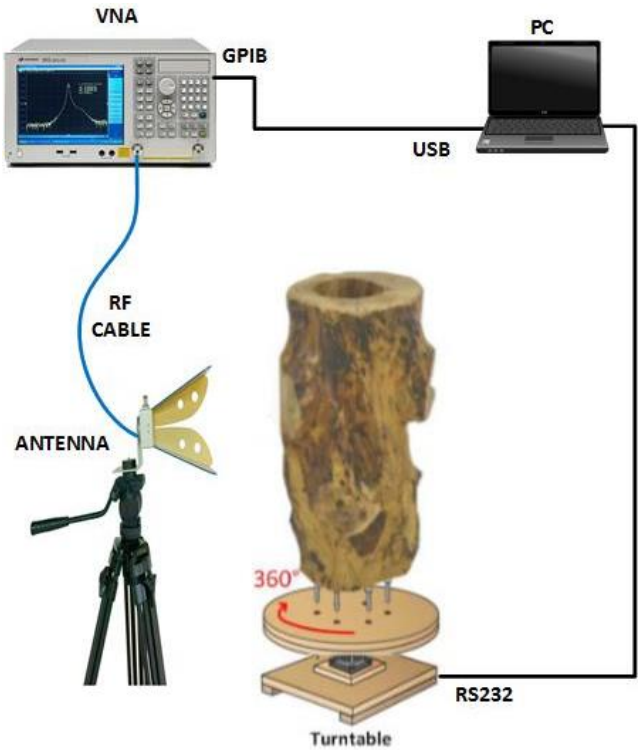

Figure 4. The measurement set-up for tree-trunk imaging experiment

For the presented configuration in Fig. 4, a piece of pine tree trunk with outer-diameter of approximately 40 cm was used as the target to be imaged. 40 cm in diameter for a tree-trunk is reasonable for operation purposes since smaller diameter trees usually present comparatively much lesser danger by falling onto people, houses and cars. The tree has a cavity whose center is

about 5 cm away from the center of the tree with diameter about 7cm-11cm as pictured in Fig. 5 (a), (b), respectively. The experiment was performed with the measurement test-bed in our anechoic chamber of MEATRC facility. During this experiment, the tree trunk whose picture is seen in Fig. 5 was put on the turn table. The antenna in monostatic configuration was positioned 36 cm away from the perimeter of tree trunk as seen in Fig. 5. The antenna position must be as close as to the tree's surface for a better penetration and therefore imaging. Antenna has a length of 32 cm and antenna's feeding point that is the phase center of imaging is about 40 cm away from the tree's surface such that antenna do not touch the tree surface while circular scanning of arbitrarily shaped perimeter of the tree. By using the automation software that was adopted by our Matlab script, turn table has been turned fast for the full azimuth coverage of 360° at 1° increments which was adequate for better imaging quality and resolution. If the step size of data collection is increased, the quality and resolution of focusing images would be decreased. For each look-angle measurement, the frequency of the VNA was varied from 1 to 8 GHz for a total of 100 discrete frequency points as in the case of the simulation. 1-8 GHz frequency range was selected to have a better resolved image due to ultra-wide band operation. Therefore, a 2D scattered electric-field matrix; $\boldsymbol{E^s}(k,\emptyset)$ of 100×360 measurement data points were collected. Theoretical achievable resolution is calculated as $\Delta r = \frac{c}{(2*B*\sqrt{\epsilon_r})} = 1.66$ cm for the bandwidth of $B = 7\ GHz$ which is approximately maximum bandwidth capacity for our VNA used for the experiment. Measured relative electric permittivity of tree trunk; ϵ_r is about 1.65 for the whole bandwidth. Then, 2D range-aspect data $\boldsymbol{E^s}(r,\emptyset)$ were obtained by applying the IFT operation along the frequency axis as plotted in Fig 6 (a). As it can be seen from the figure that the scattering from the tree's body is in the form of a wavy sinusoidal line around 36 to 40 cm due to the tree's body's perimeter do not offer a uniform circle; rather an arbitrary shape. We also notice the scattering from cavity that experience the same behavior of the tree's body as the look angle varies during the measurement. The disturbance of the scattering energy due to existence of the cavity is realized but its intensity is much weaker than the simulation because of the higher attenuation inside the tree body. Afterwards, the CBPA was applied to migrate the data from range-aspect domain to the image domain. The final TIIR image was obtained as result of the algorithm as pictured in Fig. 6(b). Thanks to the focusing ability of CBPA, the tree trunk's interior image was successfully formed. We can easily notice the borders of impedance changes from air to tree-body and tree-body to cavity and vice versa. The resultant TIIR images also shows us the geometry of tree-body and the cavity around their locations such that the cavity inside the tree-trunk is correctly detected and imaged.

Figure 5. (a) Side view picture of the tree trunk inside cavity at experiment, (b) Top view picture of the tree trunk inside cavity at experiment.

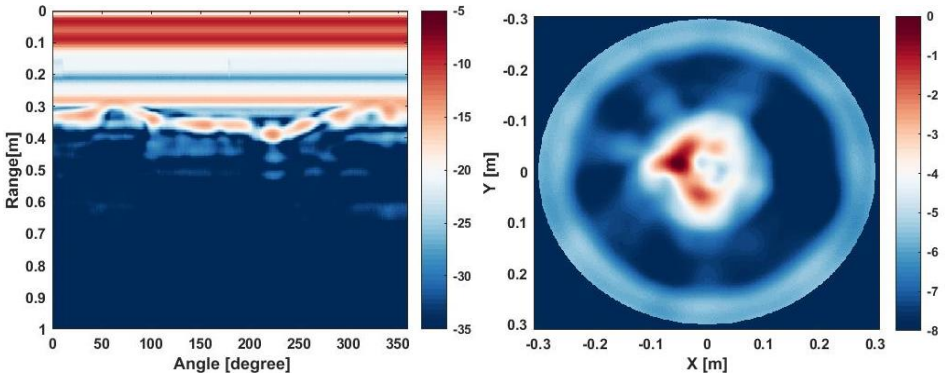

Figure 6. Measured results for the experiment: (a) Measured range-angle data, and (b) measured TIIR image

5. CONCLUSION

In this study, we have developed an algorithm to image tree trunk's interior region with help of a SFCW radar by measuring and processing the backscattered electric field from the tree body. We have implemented and employed the CBPA to the TIIR problem. In this work, the CPBA was specially developed for multi-angle multi-frequency monostatic radar set-up with circular scanning geometry of TIIR problem. The details of the algorithm were given together with the assumptions during the employment of the procedure. The algorithm was initially tested with the simulation data in which the hypothetic cavities inside the virtual tree body have been perfect detected successfully at their exact locations. Then, an experiment was conducted at Mersin University's MEATRC facility to assess the availability of the proposed technique in real world applications. It is demonstrated that the cavity inside real tree trunk was also detected and located effectively using the algorithm. Thereby, both the simulated and the measured image results show the validity and the success of the proposed method in detecting and localizing the cavity regions inside the tree body.

In the future study, the velocity changes of the electromagnetic waves inside the tree-body should be taken into account to improve the detecting capability of the proposed technique. This algorithm can also be applied similar problems such as detecting and imaging breast tumors by employing a similar geometry for the data collection.

Acknowledgments

This work has been funded by Mersin University Scientific Research Project Unit with grant no: BAP 2015-TP3-1158. The authors are also thankful to Mersin University MEATRC management for their help and support while conducting the experiments.

REFERENCES

[1] A. Brookes. (2007) Preventing death and serious injury from falling trees and branches, Australian Journal of Outdoor Education, 11(2), 50-59.

[2] J. Watt and D. J. Ball. (2009) Trees and the Risk of Harm, Report for the National Tree Safety Group.

[3] V. Bucur. (1995) Acoustics of Wood. CRC Press, Boca Raton, FL.

[4] S.A. Al Hagrey. (2006) Electrical resistivity imaging of wooden tree trunks," Near Surface Geophysics, vol. 4, 177-185.

[5] G. Catena, M. Catalano, and L. Palla. (1990) Thermal infrared detection of cavities in trees," European Journal of Forest Pathology, 20, 201–210.
[6] H. Berndt, A.P. Schniewind, G.C. Johnson. (2000) Ultrasonic energy propagation trough wood: where, when, how much, Proc. Of 12th Int. Symposium on NDT of Wood, Sopron 13-15, 57-66.
[7] M. Hasegawa, M. Takata, J. Matsumara and K. Oda. (2011) Effect of wood properties on within-tree variation in ultrasonic wave velocity in softwood, Ultrasonics 51, 296-302.
[8] J. R. Butnor, J. A. Doolittle, L. Kress, S. Cohen and K. H. Johnsen. (2001) Use of ground-penetrating radar to study tree roots in the southeastern United States, Tree Physiology 21, 1269–1278.
[9] C. Özdemir, Ş. Demirci, E. Yiğit and B. Yılmaz. (2014) A Review on Migration Methods in B-scan Ground Penetrating Radar Imaging, Mathematical Problems in Engineering, Volume,1-16.
[10] B. Yılmaz, Ş. Demirci, E. Yiğit and C. Özdemir. (2013) An Experimental Study of Through-the-Wall Radar for Life sign Detection, Proceedings of Progress in Electromagn, Research Symposium (PIERS 2013),1602-1604.
[11] M. G. Amin, Through-the-Wall Radar Imaging. (2010) Taylor and Francis, Bocaraton, FL, 2010.
[12] N.J. Redding and G.N. Newsam. (2001) Inverting the Circular Radon Transform," DTSO Research Report DTSO-RR-0211.
[13] L.Zhou, C.Huang and Y.Su. (2012) A Fast back projection algorithm based on cross correlation for GPR imaging," IEEE Geoscience and Remote Sensing Letters, vol.9, no.2, pp.228-232.
[14] H.Zhang, S.Ouyang, G.Wang, J.Li, S.Wu and F.Zhang. (2015) Back projection algorithm based on self correlation for ground penetrating radar imaging, Journal of Applied Remote Sensing, vol.9, 095059.
[15] S.Sardar and A.K.Mishra. (2011) "A UBW based Improved Imaging of Breast Tumors," IEEE Applied Electromagnetics Conference (AEMC). DOI: 10.1109/AEMC.2011.6256909
[16] D.Oloumi, P. Boulanger, A.Kordzadeh and K. Rambabu.(2015) Breast Tumor Detection Using UWB Circular-SAR Tomographic Microwave Imaging, IEEE 37th Annual International Conference in Medicine and Biology Society (EMBC). DOI: 10.1109/EMBC.2015.7320019
[17] B. Yılmaz, C. Özdemir and S. Gökkan. (2016) A focusing algorithm for tree-penetrating radar imaging: An experimental study and concept evaluation, Radar Symposium (IRS), 2016 17th International, Krakow, Poland.
[18] C. Özdemir. (2012) Inverse Synthetic Aperture Radar Imaging with Matlab Algorithms, John Wiley & Sons, Hoboken, NJ, USA.
[19] R. Bhalla, J. Moore and H. Ling. (1997) A global scattering center representation of complex targets using the shooting and bouncing ray technique," IEEE Trans. Antennas Propagat., vol. 45, pp. 1850–1856.
[20] C. Özdemir, R. Bhalla, H. Ling. (2000) A radiation center representation of antenna radiation patterns on a complex platform," IEEE Trans. Antennas Propagat., 48, 992-1000.
[21] D. J. Daniels, Surface-Penetrating Radar, IEEE Press, 1996.
[22] R. Mersereau and A. Oppenheim. (1974) Digital reconstruction of multidimensional signals from their projections, Proceedings of the IEEE, vol. 62, no. 10, pp. 1319–1338.
[23] MATLAB, R2015a, MathWorks Inc., Natick, MA, 2015.